*Proc. of the European Safety and Reliability Conference (ESREL 2026)*
*Edited by* José C. Matos, Paulo B. Lourenço, Michael Beer, Daniel Oliveira, Edoardo Patelli, Hélder S. Sousa, Rui A. Silva and Monica Santamaria

doi: 10.3850/ESREL2026061419_esrel26-p26583-cd

# Vulnerability of existing rockfall protection galleries

Kristian Schellenberg, Alexander Kagermanov

*Equi Bridges Ltd., Chur, Switzerland. E-mail: kristian.schellenberg@equibridges.ch, alexander.kagermanov@equibridges.ch*

Yoshiki Oikawa, Yusuke Kurihashi

*Kanazawa University, Kanazawa, Japan. E-mail: yoshiki@stu.kanazawa-u.ac.jp., kuri@se.kanazawa-u.ac.jp*

In Switzerland, the guideline for the design of rockfall protection galleries has been revised with the aim of accounting for the structural dynamic behaviour, the probability of failure, and the acceptable risk levels associated with uncertainties in predicting the impacting rock mass and velocity. The introduction of calibration factors enables the straightforward application of static equivalent impact forces together with the current national structural codes. Different factors are proposed according to acceptable risk levels, considering consequences, cost efficiency, and the level of confidence in the prediction of loading, to improve the level of protection. The purpose of this approach is to promote the assessment of existing structures using this methodology and to demonstrate its applicability to other types of loading scenarios. The vulnerability curves of galleries were evaluated using a nonlinear dynamic finite element tool (XDEEA) and validated through comparisons with existing studies (LS-DYNA analyses and experimental data). Pushover analyses were carried out by increasing the impact velocity until a defined failure criterion was reached. Based on the generated vulnerability curves, the loading conditions were incrementally increased until the target reliability indices were achieved, depending on the assumed uncertainties. As a result, calibration factors consistent with the social importance (consequences) of the gallery and the desired structural performance level were obtained. The resulting correction factors in comparison to the current design guideline demonstrate the potential of a performance-based design approach while maintaining a simple and practical design methodology for engineers. The presented approach can also be applied to other loading conditions.

*Keywords*: existing *protection gallery, finite element method, target reliability, uncertainties, vulnerability curve, correction factor*

## 1. Introduction

In mountainous regions, rockfall protection galleries are widely used to ensure the safety of road and railway infrastructure. Conventional design approaches generally rely on static equivalent impact forces derived from representative values of rockfall mass and velocity. Although this approach is simple and practical, it does not explicitly account for the inherent uncertainties of rockfall phenomena or the nonlinear and dynamic response of the structure.

Rockfall characteristics such as mass, velocity, and impact location exhibit significant variability due to local topography and geological conditions, while the structural response involves complex nonlinear behavior and potential failure mechanisms. As a result, deterministic design based on a single characteristic load may be overly conservative or may not clearly relate the applied load to the required performance level, particularly when assessing existing structures where acceptable risk and societal consequences are not explicitly addressed.

To overcome these limitations, Switzerland has recently revised its design guidelines for rockfall protection galleries by introducing a reliability- and performance-based framework. While retaining the use of static equivalent impact forces for practical design, the guidelines incorporate a calibration factor (C-factor) to account for structural dynamics, failure probability, and uncertainties in loading. The C-factor is defined as a correction factor linking the dynamic impact force to an equivalent static design load and is specified according to target reliability indices corresponding to acceptable risk levels.

In the current ASTRA guideline, C-factors are prescribed within a relatively wide range (typically 0.4 or 1.2). However, the basis for selecting an appropriate value within this range, and its explicit relationship to structural importance and uncertainty in rockfall characteristics, remains insufficiently defined. This lack of transparency motivates the need for a more rational and systematic derivation of C-factors grounded in reliability and performance considerations.

The present study focuses on the conceptual framework established by the revised Swiss guideline and aims to clarify the role of calibration factors through a reliability- and performance-based assessment of rockfall protection galleries. By employing nonlinear dynamic analysis to characterize structural vulnerability, this work seeks to demonstrate how the guideline's philosophy can be systematically interpreted and applied in engineering practice.

## 2. Simplified Methodology for Updating the ASTRA 12006 C-Factors

The simplified methodology for updating the ASTRA 12006 [ASTRA 2008] C-factors consists of the following steps [Schellenberg et al. 2011]:

(i) Select a prototype gallery (geometry, material properties, reinforcement and cushion layer)

(ii) Determine the structural resistance according to the design code SIA262:2013 P(R).

(iii) Calculate the vulnerability curve (mass-velocity failure values) using dynamic analysis

(iv) Select a safety level, i.e. a target reliability index $\beta_T$

(v) Obtain ($m_k$, $v_k$) values for a given return period corresponding to $\beta_T$

(vi) Calculate the equivalent static impact force $F_k(m_k,v_k)$ according to ASTRA 12006

(vii) Calculate the updated C-factor as:

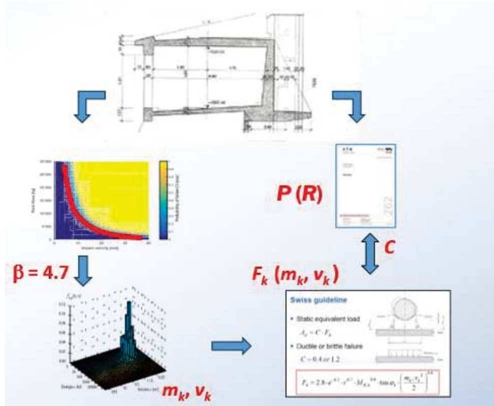


Fig. 1. Simplified methodology for updating the ASTRA12006 C-factors

$$C = A_d / F_k \qquad (1)$$

The selection of the reliability index, β, depends on several factors, such as traffic volume, importance of the road, cost of rehabilitation and consequences of collapse. The values proposed in the Swiss Code for existing structures SIA269 Table 1 are used in the present study.

Table 1 *Target reliability indexes with reference to 1 year (SIA269)*

| Massnahmeneffizienz $EF_M$ gemäss Ziffer 5.4 | Konsequenzen eines Tragwerksversagens gemäss (9) | | |
|---|---|---|---|
| | gering $\rho < 2$ | moderat $2 < \rho < 5$ | gross $5 < \rho < 10$ |
| klein: $EF_M < 0{,}5$ | 3,1 | 3,3 | 3,7 |
| mittel: $0{,}5 \le EF_M \le 2{,}0$ | 3,7 | 4,2 | 4,4 |
| gross: $EF_M > 2{,}0$ | 4,2 | 4,4 | 4,7 |

## 3. Riienertobel (existing gallery)

### 3.1. *Dynamic FE modell*

The FE-Modell was based on the information published in "Failure Probability for Extreme Load Cases evaluated by FE-calculations – A Case Study for the Rockfall Protection Gallery Riienertobel" by Kurihashi et al. In this paper, a detailed FE-model was created with LS-Dyna. In order to reduce computational efforts, a simpler approach based on shell elements and nonlinear springs implemented in the FE-Software XDEEA is used. As shown in section 3.2.2, the model shows comparable accuracy to LS-Dyna. The computational time is by factor of 100 faster. In addition, a refined failure criteria based on SIA for punching is introduced, which could not be adequately captured with LS-Dyna. A summary of the FE-Modell is provided below.

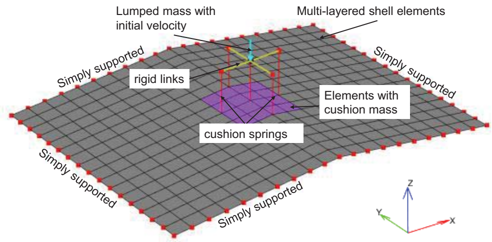


Fig. 2. *Dynamic FE Modell of Rieinertobel*

### 3.1.1. *Slab*

The slab of the gallery represents the critical component of the structure. It is modelled with nonlinear shell elements consisting of multiple layers across the thickness. The layers are used to assign different material properties, i.e. concrete and steel. The constitutive model for concrete is based on the compression field theory. For steel, a uniaxial elasto-plastic model with strain-hardening is used. The following parameters are assumed:

Concrete compressive strength $f_{cd}$ = 41.2 MPa

Reinforcement yield strength $f_{sd}$ = 290 MPa

The slab is assumed as simply supported. The influence of columns and transverse beams is neglected. For the permanent loads, a value of 14.15 kN/m$^2$ is adopted.

### 3.1.2. *Cushion layer and rock impact*

The stiffness and strength of the cushion layer is represented by five compression-only springs attached to the rock by means of rigid links. The distance between springs is based on the 30° projection of the rock through the cushion layer, as suggested in the current ASTRA12006, and 45° through the slab. Based on the Kurihashi et al. the following parameters are assumed:

Thickness of cushion Layer $e$ = 30 cm

Self-weight of cushion Layer $\gamma$ = 18 kN/m$^3$

The backbone curve is defined by three parameters: the initial stiffness $a = EA/ne$ (kN/m), peak strength $b = \sigma A/n$ (kN), and post-peak stiffness $c = 0.05\ a$ (kN/m). Here, $E$ denotes the elastic modulus of the cushioning layer (MPa), $\sigma$ denotes the compressive strength of the cushioning layer (MPa), $n$ is the number of springs, $A$ is the projected area of the falling rock (m²), and $e$ represents the thickness of the cushioning layer (m).

### 3.1.3. *Mass and damping*

In order to perform the dynamic analysis in time-domain, a definition of mass and damping is required. For the mass of the slab, only the self-weight and a portion of the cushion layer located within the rock projection is considered. The mass of the rock is lumped at the centroid, assuming an equivalent sphere. Hysteretic damping due to material dissipation is considered in the constitutive models. Viscous damping due to additional damping sources is modelled as Rayleigh damping (initial mass and stiffness proportional) with a value of 8%.

### 3.1.4. *Failure criteria*

Flexural failure is verified based on material strains obtained from SIA262. The yield strain of reinforcing steel was taken as $\varepsilon_{sy}$ = 2500μ, the ultimate strain as $\varepsilon_{su}$ = 25000μ, and the compressive strain of concrete as $\varepsilon_{cu}$ = 3500μ.

Shear in the vicinity of wall and beam supports is verified based on the SIA262 design equations as:

$$v_{Ed} \leq v_{Rd} \tag{2}$$
$$v_{Rd} = k_d\ \tau_{cd}\ d_v \tag{3}$$

where $v_{Ed}$ is the applied shear obtained from dynamic FE analysis, $v_{Rd}$ the resisting shear, $k_d$ the reduction factor considering the opening of flexural cracks, $\tau_{cd}$ the nominal shear stress and $d_v$ the effective depth. Since $k_d$ depends on the longitudinal strain, which varies during the analysis, also $v_{Rd}$ is time dependent.

Punching in the vicinity of the impact zone and columns are verified based on the SIA262 design equations as:

$$V_{Ed} \leq V_{Rd,C} \tag{4}$$
$$V_{Rd,C} = k_r\ \tau_{cd}\ u\ d_v \tag{5}$$

where $V_{Ed}$ is the total vertical force (integral of shear stresses along the critical perimeter), obtained from dynamic FE analysis, $V_{Rd,c}$ the punching strength, $k_r$ the reduction factor considering the opening of the critical shear crack, $\tau_{cd}$ the nominal shear stress, $d_v$ the effective depth and u the length of the critical perimeter. Since $k_r$ depends on the rotation, which varies during the analysis, also $V_{Rd,c}$ is time dependent. Note that strain-rate effects can be easily considered as an increase in strength properties.

## 3.2 *Example calculation*

### 3.2.1. *M = 10 t, v = 15 m/s*

Results from a dynamic calculation with a mass of 10 t and impact velocity of 15 m/s in the center of the slab are shown below. For the verification of the flexural limit states, the maximum concrete compressive strains and steel tensile strains are reported. Local concrete crushing occurs at the corners due to modelling assumptions and can be neglected. Steel yielding occurs in the center without exceeding the fracture strain.

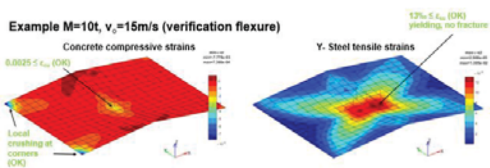


Fig. 3. Concrete compressive strains and steel tensile strains.

Punching verification was performed by plotting the total force – rotation curves against the capacity curve given as [Muttoni 2008]:

$$\frac{V_R}{b_0 d\sqrt{f_c}} = \frac{3/4}{1 + 15\frac{\psi d}{d_{g0}+d_g}} \qquad (6)$$

Where $b_0$ is the length of the critical perimeter, $d$ the effective depth, $d_{g0}$ is defined as 16 mm and $d_g$ the maximum aggregate size.

The rotation was obtained from the nodes located below the springs, which is very similar to the rotation of the points along the critical perimeter located at $0.5d_v$. The total force was obtained as the sum of the vertical spring forces. It can be seen that the capacity curve is intersected with all points, implying that punching failure occurred. A similar verification was conducted at the edges of the slab.

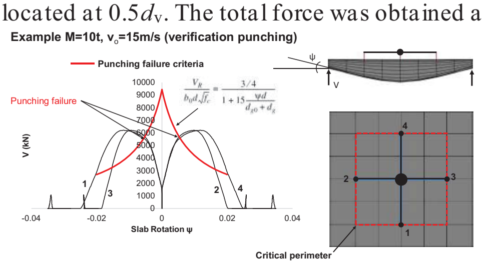


Fig. 4. *Punching verification of the force-rotation*

### 3.2.2 Comparison with LS-Dyna

The results were verified against LS-Dyna calculations reported in Kurihashi et al. 2018 for different impact velocities (10 m/s, 15 m/s, 20 m/s and 25 m/s). Displacement and impact force time histories are reported below. It can be seen that overall the model shows good agreement with LS-Dyna.

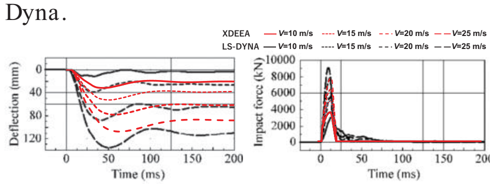


Figure 5. *Comparison with of XDEEA and LS-Dyna results*

## 4. Wandschluichen (new gallery)

### 4.1 *Dynamic FE Modell*

The Rieinertobel gallery is representative of old design practice. Modern galleries are built with thicker slabs and greater amounts of reinforcement. The Wandschluichen gallery was modelled next in order to investigate the performance of modern galleries. The gallery is supported on a retaining wall, on the mountain-side, and 50 cm square columns spaced at 5 m, on the valley-side. The slab thickness was 85 cm with ϕ30/150 mm bottom and top reinforcement in the longitudinal and transverse directions. In addition, shear reinforcement was distributed in the entire plate.

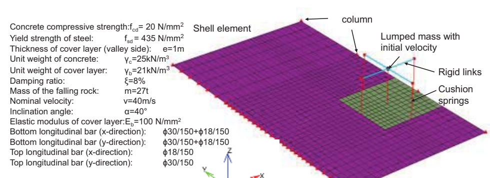


Fig. 6. Dynamic FE-Modell of Wandschluichen gallery

The FE-Modell consisted of the slab continuously supported on the mountain-side and with point supports on the valley-side. The critical location for the rock impact was near the column support. The thickness of the cushion layer at this location is 1 m. As before, the stiffness and strength of the cushion layer is represented by five compression-only springs attached to the rock by means of rigid links. Furthermore, as the cushion layer slopes from the mountain side towards the valley, a simplified model was constructed by defining distinct dead loads for each section. Below, results from a sample calculation for $m = 27$ t and $v = 25.7$ m/s are reported.

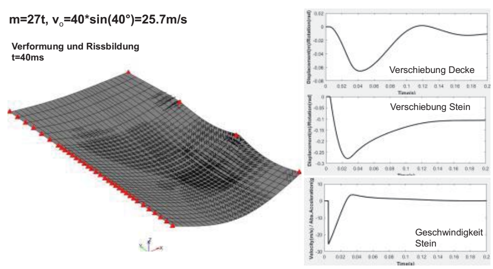


Fig. 7. Sample dynamic calculation

### 4.2 Vulnerability curves

The vulnerability curve for the case of rock impact near support is compared with the results for Rieinertobel (Fig 8.). In the calculation, the influence of punching reinforcement on the resistance was neglected. Also, only punching failure of the rock through the slab was considered, since punching of the column seems to be a design deficiency of this specific gallery.

Moreover, the presence of punching reinforcement ($\phi$12/20 within 0.35$d$ - $d$ from the critical perimeter SIA262:2013) was taken into account, which is shown as dashed purple curve. For small masses and high velocities failure of the concrete struts was found to be critical.

Furthermore, the influence of the slab thickness $t$ = 60cm was investigated, which is shown as solid purple line, while keeping the rest of parameters constant. As expected, lower resistance is obtained.

## 5. Target Safety Level

Characteristic mass and velocities used for the calculation of C factors are obtained from intersection between loading and vulnerability

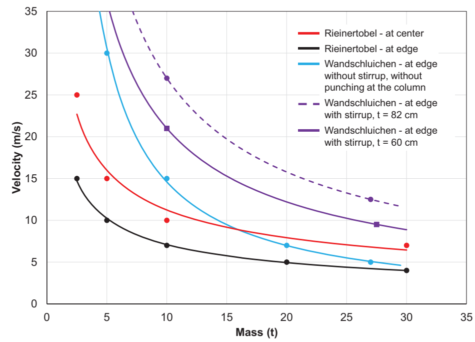


Fig. 8. Vulnerability curves: Rieinertobel and Wandschluichen position near support with punching reinforcement for thicknesses 82cm and 60cm

curves ("pushover analysis") until reaching the target reliability index, or equivalently, failure probability.

The pushover analysis is performed in the mass-velocity domain as follows. For a given mass, the shape of the loading surface can be defined from the mass and velocity dispersions, which are a function of the $m_{100}/m_{30}$ and $v_{95}/v_{50}$ ratios. Here, $m_{100}$ denotes the rockfall mass corresponding to a 100-year return period (t), $m_{30}$ denotes the rockfall mass corresponding to a 30-year return period (t), $v_{95}$ denotes the 95th percentile value of the rockfall velocity distribution, and $v_{50}$ denotes the mean value of the rockfall velocity distribution. These ratios are selected based on typical predicted values of rockfall mass and velocity obtained in practical engineering projects, and $m_{100}/m_{30}$=1.5, 2.0, $v_{95}/v_{50}$ =2.0, 3.0 are selected.

Afterwards, the velocity is increased until intersecting the vulnerability curve and reaching a determined target reliability index. The marginal distributions of both rockfall mass and velocity are modelled using Weibull distributions and are assumed to be statistically independent.

For a given distribution, four safety levels are calibrated.

(i) New gallery:
   a. National road (e.g. β=4.7)
   b. Local road (e.g. β=4.4)

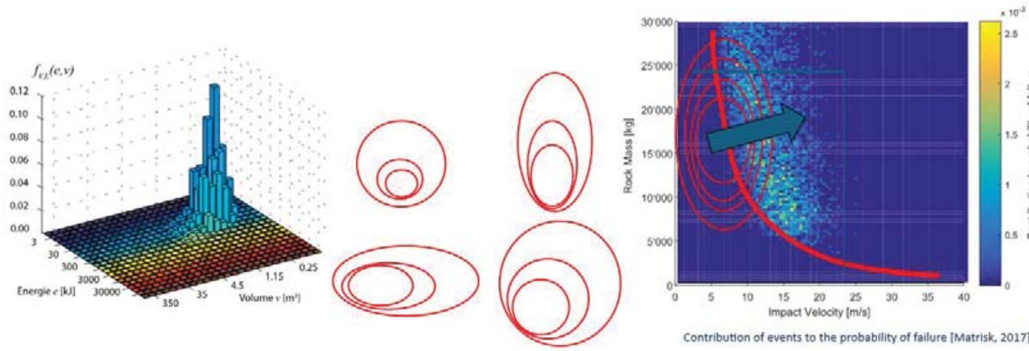


Fig. 9. *Pushover analysis framework in the mass–velocity domain with loading uncertainties*

(ii) Existing gallery
  a. National road (e.g. β=3.7)
  b. Local road (e.g. β=3.3)

Different loading shapes are possible depending on the uncertainties in mass and velocity ratios (Figure 9): (i) large uncertainties in rock mass, (ii) large uncertainties in rock velocity or (iii) large uncertainties in both. In other words, β, mass ratio, and velocity ratio are to be parameter in the pushover analysis. 30t mass truncation is applied due to practical and physical limitations.

To evaluate the influence of resistance uncertainty, a simplified sensitivity analysis was conducted. In this analysis, the effect of material variability was represented by reducing the static resistance by 20%, which is equivalent to increasing the impact force by a factor of 1.2. The results indicate that, although minor differences in the resulting C-factors can be observed, the overall trend and conclusions of the study remain unchanged. Therefore, the influence of material uncertainty is considered secondary compared to the variability in rockfall loading. Based on this observation, the assumption of neglecting resistance uncertainty is considered reasonable within the scope of this study.

## 6. Determination of C-factor

### 6.1. *Rock impact force $F_k$*

In the new guidline, the rockfall impact force is given by Equation (7), where $F_k$ denotes the characteristic value of the impact force at the point of contact, $m_k$ denotes the characteristic value of the rockfall mass, $v_k$ denotes the characteristic value of the impact velocity, $r$ denotes the rockfall radius, $e$ denotes the thickness of the cushioning layer, $M_{E,k}$ denotes the characteristic value of the elastic modulus of the cushioning material, and $\varphi_k$ denotes the characteristic value of the friction angle of the cushioning material.

By substituting the values of $m_k$ and $v_k$ obtained in Section 5 into Eq. (7), the impact force can be evaluated while accounting for the uncertainty associated with rockfall characteristics.

$$F_k = 2.8 \cdot e^{-0.5} \cdot r^{0.5} \cdot M_{E,k}{}^{0.4} \cdot \tan\varphi_k \cdot \left[\frac{m_k \cdot v_k{}^2}{2}\right]^{0.6} \quad (7)$$

In appendix A and B, there are tables that shows the one of the example results obtained by pushover analysis and by substituting $m_k$ and $v_k$ into Eq. (7)

### 6.2. Calculation of C-factor

By substituting the impact force $F_k$ obtained in Section 6.1 into Eq. (1), the calibration factor C can be derived. $P$(R) represents the static load equivalent to the impact force $F_k$. In this study, $P$(R) is regarded as the static ultimate resistance, which enables an equivalent evaluation of the calibration factor C.

The value of $P$(R) is calculated in accordance with SIA 262, and the resistance considered depends on the loading condition of the rockfall that flexural resistance is used for central loading, whereas shear resistance is adopted for edge loading.

The final results of the calibration factor C proposed in this study are summarized in the table below. In addition, examples of the calculated C values are presented in tabular form in the Appendix C. The C-values presented in Appendix C represent intermediate results obtained for specific parameter combinations and are provided for illustration purposes only. The recommended C-factor range for design is summarized in Table 3. C-factor that is taken for the results is maximum value in order to consider the conservative side.

Table 3 *Final results of C-factor*

| | $m = m_{100}/m_{30}$ | New construction | | Existing gallery | |
|---|---|---|---|---|---|
| Uncertainty in rock velocity | Uncertainty in rock mass | National road (β = 4.7) | Local road (β = 4.4) | National road (β = 3.7) | Local road (β = 3.2) |
| $v_{95}/v_{50} < 3$ | < 2 | 0.55 (0.60) | 0.42 (0.50) | 0.33 (0.40) | 0.26 (0.30) |
| | > 2 | 0.57 (0.65) | 0.42 (0.55) | 0.33 (0.45) | 0.27 (0.35) |
| $v_{95}/v_{50} > 3$ | < 2 | 0.72 (0.75) | 0.53 (0.65) | 0.37 (0.50) | 0.25 (0.40) |
| | > 2 | 0.72 (0.80) | 0.54 (0.70) | 0.39 (0.55) | 0.27 (0.45) |

As shown in Table 3, the proposed C factors are more flexible and generally smaller than the values specified in the current guideline, indicating that a more rational design can be achieved by explicitly considering both the structural importance and the uncertainty associated with rockfall characteristics.

## 7. Conclusions

The main findings of this study are summarized as follows:

(i) Two representative galleries (existing and new) were analysed using nonlinear dynamic FE models. A simplified modelling approach with shell and spring elements achieved high accuracy with reduced computational cost, enabling the derivation of multiple vulnerability curves for different impact scenarios.

(ii) A reliability-based simplified methodology was proposed to derive C-factors considering uncertainties in rock mass and velocity. The resulting C-factors (0.3–0.8) enable linear static design with equivalent impact forces while accounting for dynamic effects and acceptable risk levels.

(iii) The proposed design framework allows different target reliability levels depending on gallery and road importance. Accurate estimation of rockfall mass and velocity distributions, based on a 30-year return period, is essential and may require project-specific operational measures.

The applicability of the proposed methodology is currently limited to the investigated gallery types and loading conditions. Although the framework itself is general, the calibrated C-factors should be applied with caution to significantly different structural configurations, impact conditions, or geological environments. Further validation using a broader range of case studies is required to enable a more comprehensive and careful assessment.

**Acknowledgement**

The authors gratefully acknowledge Matrisk GmbH for performing the probabilistic analyses used in this study.

**Appendix A. Example table of characteristic rockfall velocity $v_k$ (m/s) obtained from the pushover analyses (Riienertobel gallery, central rockfall impact, mratio = 2.0, vratio = 3.0).**

| β | Characteristic mass value $m_k$ (t) | | | | | | | | | | | |
|---|---|---|---|---|---|---|---|---|---|---|---|---|
| (-) | **12.8** | **18.3** | **20.8** | **22.1** | **23** | **23.5** | **24** | **24.3** | **24.6** | **24.8** | **25** | **25.1** |
| 3.2 | 5.93 | 5.26 | 4.96 | 4.76 | 4.64 | 4.7 | 4.56 | 4.56 | 4.46 | 4.52 | 4.48 | 4.43 |
| 3.7 | 4.37 | 3.92 | 3.81 | 3.69 | 3.72 | 3.62 | 3.57 | 3.61 | 3.54 | 3.49 | 3.49 | 3.5 |
| 4.2 | 3.45 | 3.13 | 3.06 | 3.01 | 2.97 | 2.93 | 2.9 | 2.91 | 2.88 | 2.86 | 2.85 | 2.84 |

| | | | | | | | | | | | | |
|---|---|---|---|---|---|---|---|---|---|---|---|---|
| 4.7 | 2.8 | 2.59 | 2.53 | 2.47 | 2.45 | 2.42 | 2.41 | 2.4 | 2.37 | 2.39 | 2.39 | 2.39 |

**Appendix B. Example table of characteristic impact force $F_k(m_k, v_k)$ (kN) obtained using the ASTRA formula from the combinations of $m_k$ and $v_k$ in Appendix A.**

| β | Average of mass value $m_{ave}$ (t) | | | | | | | | | | | |
|---|---|---|---|---|---|---|---|---|---|---|---|---|
| (-) | 2.5 | 5 | 7.5 | 10 | 12.5 | 15 | 17.5 | 20 | 22.5 | 25 | 27.5 | 30 |
| 3.2 | 7991 | 9298 | 9636 | 9666 | 9679 | 10024 | 9826 | 9928 | 9750 | 10002 | 9954 | 9861 |
| 3.7 | 5543 | 6532 | 7025 | 7116 | 7410 | 7326 | 7331 | 7515 | 7391 | 7327 | 7365 | 7430 |
| 4.2 | 4182 | 4997 | 5389 | 5565 | 5652 | 5684 | 5695 | 5791 | 5771 | 5772 | 5777 | 5779 |
| 4.7 | 3255 | 3975 | 4294 | 4389 | 4496 | 4530 | 4561 | 4594 | 4569 | 4661 | 4679 | 4693 |

**Appendix C. Example of intermediate C values using Appendix B (for illustration only).**

| β | Average of mass value $m_{ave}$ (t) | | | | | | | | | | | |
|---|---|---|---|---|---|---|---|---|---|---|---|---|
| (-) | 2.5 | 5 | 7.5 | 10 | 12.5 | 15 | 17.5 | 20 | 22.5 | 25 | 27.5 | 30 |
| 3.2 | 0.07 | 0.06 | 0.06 | 0.06 | 0.06 | 0.05 | 0.06 | 0.06 | 0.06 | 0.05 | 0.06 | 0.06 |
| 3.7 | 0.1 | 0.08 | 0.08 | 0.08 | 0.07 | 0.08 | 0.08 | 0.07 | 0.07 | 0.08 | 0.07 | 0.07 |
| 4.2 | 0.13 | 0.11 | 0.1 | 0.1 | 0.1 | 0.1 | 0.1 | 0.09 | 0.1 | 0.1 | 0.1 | 0.1 |
| 4.7 | 0.17 | 0.14 | 0.13 | 0.13 | 0.12 | 0.12 | 0.12 | 0.12 | 0.12 | 0.12 | 0.12 | 0.12 |

## References


ASTRA/SBB, (1998), “Einwirkung auf Steinschlagschutzgalerien“, Richtlinie, Bundesamt für Strassen, Baudirektion SBB, Eidgenössische Drucksachen- und Materialzentrale, Bern.

ASTRA 82006, (2003), “'Steinschlag': Naturgefahr für die Nationalstrassen“, Schlussbericht, ASTRA-Expertengruppe.

ASTRA, SBB, (2008), “Einwirkungen infolge Steinschlags auf Schutzgalerien“, Richtlinie Ausgabe 2008, V2.03, Bundesamt für Strassen, in Zusammenarbeit mit SBB AG Infrastruktur, 22 pp. www.astra.admin.ch

Muttoni A., (2008) “Punching Shear Strength of Reinforced Concrete Slabs
without Transverse Reinforcement” ACI Structural Journal, V. 105, No. 4, July-August 2008.

Kurihashi Y., Komuro M., Schubert M., Custer R., Schellenberg K. “Failure Probability for Extreme Load Cases evaluated by FE-calculations – A Case Study for the Rockfall Protection Gallery Rieinertobel”

Röthlin C., Vogel T., Custer R., Schubert M., “Grundlagen zur Überprüfung und Bemessung von Steinschlagschutzgalerien“ ASTRA Bericht 697, Forschungsauftrag AGB 2011/014

Schellenberg, K. (2008), “On the design of rockfall protection galleries“, Institut für Baustatik und Konstruktion, ETH Zürich, IBK Bericht Nr. 334, Dissertation Nr. 17924, Zürich, 2008, 177 pp.

Schellenberg, K., and Vogel, T., (2009), “A dynamic design method for rockfall protection galleries”, Structural Engineering International, Vol. 19, No. 3, 2009, 321-326 pp.

Schellenberg K, Schubert M, Vogel T. 2011, “A performance based design concept for rockfall protection galleries“, Proceedings, 9th International Conference on Shock & Impact Loads on Structures; Nov 16-18, 2011; Fukuoka, Japan

SIA 260 (2013), “Grundlagen der Projektierung von Tragwerken“, Schweizer Norm 505 260, Schweizerischer Ingenieur- und Architektenverein, Zürich, 2013, 44 pp.

SIA 261 (2014), “Einwirkung auf Tragwerke“, Schweizer Norm 505 261, Schweizerischer Ingenieur- und Architektenverein, Zürich, 2013, 132 pp

SIA 262 (2013), “Betonbau“, Schweizer Norm 505 262, Schweizerischer Ingenieur- und Architektenverein, Zürich, 2013, 102 pp.

SIA 269 (2011), “Grundlagen der Erhaltung von Tragwerken“, Schweizer Norm 505 269, Schweizerischer Ingenieur- und Architektenverein, Zürich, 2013, 28 pp.